Received: 4 May 2017 | Revised: 30 June 2017 | Accepted: 4 July 2017

DOI: 10.1002/jbio.201700111

Journal of BIOPHOTONICS

FULL ARTICLE

In vivo THz imaging of human skin: Accounting for occlusion effects

Qiushuo Sun | Edward P.J. Parrott | Yuezhi He | Emma Pickwell-MacPherson*

Department of Electronic Engineering, The Chinese University of Hong Kong, Shatin, NT, Hong Kong

*Correspondence
Emma Pickwell-MacPherson, Department of Electronic Engineering, The Chinese University of Hong Kong, Shatin, NT, Hong Kong.
Email: emma@ee.cuhk.edu.hk

Funding information
Research Grants Council of Hong Kong, Grant/Award number: 415313 and 14205514; Hong Kong PhD Fellowship

In vivo terahertz (THz) imaging of human skin needs to be done in reflection geometry due to the high attenuation of THz light by water in the skin. To aid the measurement procedure, there is typically an imaging window onto which the patient places the area of interest. The window enables better pulse alignment and helps keep the patient correctly positioned during the measurement. In this paper, we demonstrate how the occlusion caused by the skin contact with the imaging window during the measurement affects the THz response. By studying both rapid point measurements and imaging over an area of a human volar forearm, we find that even 5 seconds of occlusion affects the THz response. As the occlusion time increases, the skin surface water content increases, resulting in the reduction of the amplitude of the reflected THz pulse, especially in the first 3 minutes. Furthermore, it was found that the refractive index of the volar forearm increased by 10% to 15% after 20 minutes of occlusion. In this work, we examine and propose a model for the occlusion effects due to the quartz window with a view to compensating for its influence.

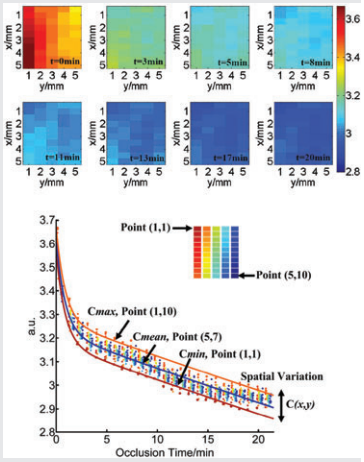

KEYWORDS
human skin, in vivo, occlusion, terahertz time-domain spectroscopy

1 | INTRODUCTION

A key feature of terahertz (THz) imaging and spectroscopy is that it can noninvasively measure properties of human skin in vivo [1]. Moreover, due to the high sensitivity of THz light to water concentration it can provide unique information that cannot be obtained by other approaches. Recently, THz in vivo imaging has shown the ability to detect scars on human bodies, even those that can barely be observed by the naked eye as the THz refractive index of the scar is clearly different from that of the surrounding skin [2]. Researchers found that THz imaging could use the water concentration in the foot to discriminate between healthy and diabetic patients, the difference being particularly significant in the greater toe area. This work shows a potential direct, objective and quantitative evaluation criteria for the early stage diagnosis of the diabetic foot [3]. THz spectroscopy has also shown promising results for early assessment (24 hours) of skin flap viability in a pilot study. As the necrotic excised flaps hold abnormally low water content in the skin, the sensitivity of THz to water content meant that local differences in tissue water content could be determined as early as 24-hour post operation using THz whereas visual images needed 48 hours [4].

Due to the high attenuation of THz light in skin, reflection geometry is the necessary geometry for in vivo THz imaging of humans. Typically, the area of interest is placed onto an imaging window; this aids with image registration, flattening the skin surface and also helps to keep the patient correctly positioned throughout the measurement [2–4]. However, the patient's skin is occluded by the imaging window; this increases the water content of the skin and will affect the THz response. This problem was first reported by Cole et al. in 2001 [5], where they evaluated the effect of skin occlusion by keeping the volar forearm in contact with the imaging window for 15 minutes and recording the THz reflection at a fixed point once every 45 seconds. They applied an exponential function to fit the reduction in amplitude of the THz response during the first 15 minutes of occlusion, yielding a time constant of 3.1 minutes. However, other variables in the skin-window contact process were not discussed and no solution was given to fix this issue. Hitherto no solution other than removing the imaging window (which introduces other problems such as pulse alignment uncertainty) has been proposed.

To determine how the imaging window affects the THz response with time, we measured volar forearms in vivo by single point scan as well as imaging an area continuously throughout 20 minutes of occlusion. In this work, we propose a model that takes the occlusion time into account as well as the spatial variation of the imaging window and skin. We also analyze the following factors: positional change of the imaging window (due to the pressure of the patient's limb), temperature changes of the window and skin, skin occlusion and the possible presence of a perspiration layer left on the window surface. Using this model we are able to compensate for the varying occlusion times that different points in the image will have endured, and thereby recover an occlusion independent image.

2 | METHODS

In our experiment, as shown in Figure 1, subjects were asked to place the area of interest, that is, the volar forearm about 5 to 10 cm away from the elbow and 2 to 4 cm away from the edge between volar and dorsal forearm (the skin near the elbow has a lower refractive index and absorption coefficient than the volar forearm in general [6]), on an imaging window (made of z-cut quartz) of a THz reflection system (Menlo Systems GmbH, Planegg, Germany). A continuous scan mode was used to measure approximately 4 scans per second for 20 minutes at a fixed point. We also imaged a 5 mm by 5 mm area 25 times throughout 20 minutes of occlusion (using a 0.5 × 1 mm resolution). Each measurement took 34 seconds to acquire, with 50 (10 points by 5 lines) usable points per measurement. In total, we measured 5 healthy subjects (3 males and 2 females, with ages between 25 and 37). The subjects exposed the area of interest to the ambient air in the THz laboratory for 20 minutes before every measurement to acclimatize to the room temperature of 21°C. A digital thermometer was used to measure the temperature of the skin surface and imaging window before and after the contact. After 20 minutes of contact, the temperature of skin decreased on average from 29°C to 26°C, while the temperature of window increased from 21°C to 26°C.

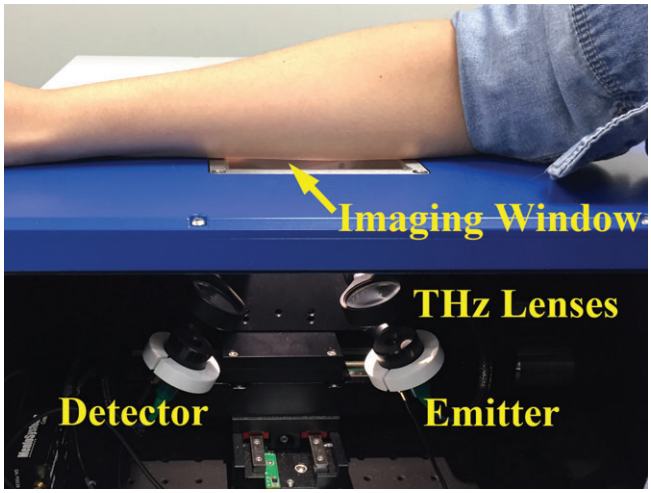

FIGURE 1 In vivo volar forearm imaging using a THz-TDS reflection spectroscopy setup

A thin layer containing products of perspiration was observed on the imaging window when the skin was removed from the window after 20 minutes of contact, which results from the trapping of insensible perspiration from the skin. To determine if this layer affected the THz response, we measured the quartz window before the skin measurement, right after removing the skin after 20 minutes of occlusion and after wiping off the perspiration layer.

The air-quartz interface and quartz-sample interface both reflect THz pulses; we define the reflections due to the former interface as the baseline and this needs to be removed from the sample information. In this study, the baseline is measured by placing another piece of quartz on the imaging window to eliminate the second pulse. The quartz-air reflection is also measured as a reference for calibration and sample characterization. Then the processed signal is computed using Eq. (1) [7, 8].

$$\text{processed signal} = i\text{FFT}\left[\text{FFT}(\text{filter}) \times \frac{\text{FFT}\left(\text{E}_{\text{sample}}(\text{t}) - \text{E}_{\text{baseline}}(\text{t})\right)}{\text{FFT}\left(\text{E}_{\text{air}}(\text{t}) - \text{E}_{\text{baseline}}(\text{t})\right)}\right] \quad (1)$$

A double Gaussian filter is selected to remove the noise in low and high frequencies with 0.1 and 0.6 THz chosen as the cut-off frequencies [9].

To further examine the occlusion effects, we extract the basic optical properties of skin and analyze the spectrum of skin. Denoting M as the ratio of the reflected sample signal $E_{\text{sample}}(\omega)$ and reference signal $E_{\text{reference}}(\omega)$:

$$M = \frac{\mathrm{FFT}\left(\mathrm{E_{sample}(t)} - \mathrm{E_{baseline}(t)}\right)}{\mathrm{FFT}\left(\mathrm{E_{air}(t)} - \mathrm{E_{baseline}(t)}\right)} \quad (2)$$

The Fresnel equations and Snell's law allow us to extract the complex refractive index of the sample by solving Eq. (3):

$$\begin{cases} M = \dfrac{r_{qs}}{r_{qa}} = \dfrac{\tilde{n}_q \cos\theta_q - \tilde{n}_s \cos\theta_s}{\tilde{n}_q \cos\theta_q + \tilde{n}_s \cos\theta_s} \cdot \dfrac{\tilde{n}_q \cos\theta_q + \tilde{n}_a \cos\theta_a}{\tilde{n}_q \cos\theta_q - \tilde{n}_a \cos\theta_a} \\ \tilde{n}_a \sin\theta_a = \tilde{n}_q \sin\theta_q = \tilde{n}_s \sin\theta_s \end{cases} \quad (3)$$

where, $\tilde{n}_a$, $\tilde{n}_q$, $\tilde{n}_s$ are the complex refractive index of air, the quartz window and sample, respectively. $\cos\theta_q$ is the incident angle in the quartz, $\cos\theta_a$ and $\cos\theta_s$ are the refraction angles in air and the sample, respectively.

3 | RESULTS AND DISCUSSION

3.1 | Time-domain results

The imaging window being used in the reflection system has a thickness 2.7 mm ± 30 μm; this thickness variation results in both the amplitude and the phase of the reflected THz signal varying with position [8, 10]. We processed the data to remove the fluctuations in the laser power and uneven thickness of the quartz window using Eq. (1). Figure 2A illustrates how the processed signal of a fixed position changes with increasing occlusion time. The curves have been translated horizontally for clarity and it is clear that the amplitude of the THz pulse reflected off the skin has decreased after 20 minutes of occlusion.

From Figure 2A, we see that the maximum and minimum of the processed signal change the most in the first 3 minutes of occlusion. We, therefore, plot the peak-to-peak (P2P) parameter for the processed signal in Figure 2B; the inset shows the reduction in the first 30 seconds. This shows that even contacting the imaging window for 5 seconds causes attenuation of the THz signal. To understand this change we consider the variables affecting the THz signal and determine which is dominant.

3.2 | Dominant variable identification

There are 4 main possible causes for the change in THz signal when the skin contacts the imaging window: the vertical downwards translation of the imaging window caused by the limb pressure, temperature change of skin and the imaging window, the formation of the perspiration products on the surface of the imaging window, and skin occlusion. So as to examine which factor dominates the change on THz response, we discuss the influence of each factor individually in this section.

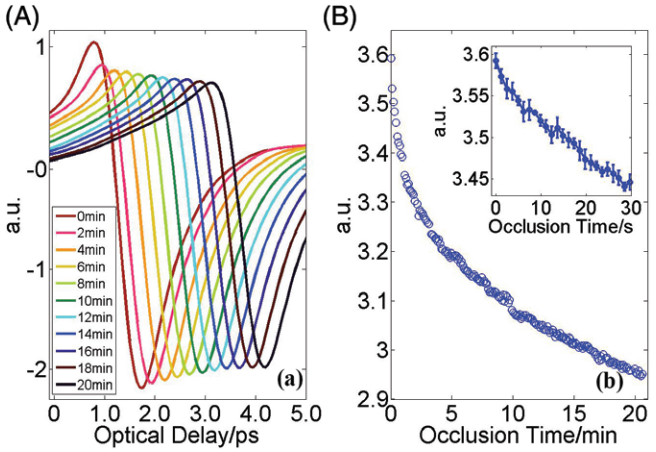

FIGURE 2 (A) Processed THz signal with different occlusion times. (B) The peak-to-peak of processed THz signal attenuates with occlusion

3.2.1 | The absolute position change of the imaging window

In our setup, the quartz window is embedded into a metal plate where the subject can put his/her arm on it. When pressure is applied to the plate, such as when a subject rests his/her limb on the imaging window, the quartz window moves vertically downwards because the quartz is more rigid than the metal around it and so the metal yields slightly. When the absolute position of the imaging window changes, the reference and sample measurements become misaligned. In addition, it is very difficult to guarantee that the sample pressure remains constant throughout the in vivo measurement. To account for these uncertainties we apply a phase-aligned algorithm recently developed by our group to eliminate this problem [10]. Briefly, this algorithm generates the reference data automatically based on the real-time power of the air-quartz reflection and the thickness of the imaging window, which has been recorded on a database before performing the sample measurements. This allows us to account for the observed position change.

3.2.2 | Temperature

Conductive heat transfer between skin and the quartz window occurs whilst in contact; consequently, the temperature of the skin surface decreases and that of the quartz window increases. The temperature increase of the quartz upper surface leads to a thermal effect, resulting in expansion of the quartz in the direction of the skin. One notable feature of quartz, however, is that it has very low thermal expansion effect with a thermal coefficient of expansion of $5 \times 10^{-7}{}^{\circ}\mathrm{C}^{-1}$ at 25°C [11]. Assuming that the quartz undergoes linear expansion vertically during the interaction with skin, the expansion length will be given by:

$$\Delta L = \alpha_{\mathrm{quartz}} \times L_0 \times (T_2 - T_1) \quad (4)$$

Here, α_{quartz} is the thermal coefficient of expansion, and L_0 is the original quartz window thickness (2.7 mm). The temperature of quartz changes from 21°C to 26°C after

20 minutes of occlusion, so the expanded change in length L is estimated to be 6.75 nm, the first equation in (3) becomes:

$$M = \frac{r_{qs}}{r_{qa}} \exp\left(-i2\frac{\Delta L}{\cos\theta_q} w \frac{\tilde{n}_q}{c}\right) \quad (5)$$

The exponential term is the phase error caused by this thermal expansion, c is the speed of light. At 1 THz, the calculated phase error is less than 0.05°, which is much less than the resolution of our THz reflection system. This result indicates that the thermal expansion of quartz is so small that it can be ignored.

To analyze the influence of temperature decrease on the skin surface, the double Debye model of water is used to simulate this change considering the similar characteristics of water and skin in the THz range [12]. According to the model proposed by Liebe et al. [13], Figure 3 shows the spectrum of refractive index of water in 0.1 to 1 THz at 29°C and 26°C, respectively. At 0.5 THz, refractive index and extinction coefficient changes of 0.5% and 1.8%, respectively, are observed, giving an upper bound on the sensitivity of skin to the temperature changes observed in the experiment which is much lower than the observed changes in our measurements.

3.2.3 | Insensible perspiration

As mentioned in section 2, we conducted 3 bare quartz window measurements: one before the skin measurement, one right after removing the arm and one after wiping away the perspiration layer. Figure 4 shows the optical properties of the "sample" measured during these 3 measurements, which should be air ($n = 1$, $\kappa = 0$), products of perspiration and air, respectively. The 3 curves overlap for the refractive index and extinction coefficient and agree closely with the expected values for air, implying that the effect of the perspiration layer can be ignored.

Therefore, skin occlusion will be the dominant factor causing the observed change to the THz response when a bio-sample is placed on the imaging window, which we focus on in the following section.

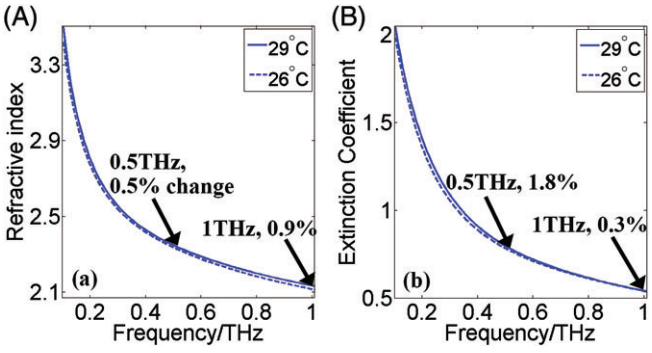

FIGURE 3 Calculated (A) refractive index and (B) extinction coefficient of water at 29°C and 26°C in 0.1 to 1 THz

3.3 | Time-domain occlusion imaging

Figure 5 shows the peak-to-peak of the processed signal for an area of skin imaged for different occlusion times. Aside from some random observable spatial variation there is also a systematic decrease in the signal peak-to-peak corresponding to the raster scan direction of the image acquisition. This systematic decrease is attributed to skin occlusion, and is most obvious in the first image due to the larger decrease in the reflected THz signal observed at short occlusion times (as shown in Figure 2).

To model this reduction in the THz response we apply a biexponential function with an amplitude term to describe the reduction as a function of occlusion time and position:

$$\text{fitted signal} = \beta_1 \exp(-t/\tau_1) + \beta_2 \exp(-t/\tau_2) + C_{(x,y)} \quad (6)$$

where,t is the occlusion time, for each subject, the constant coefficients β_1 , β_2 and reduction constants τ_1 , τ_2 are the same for all the points on the imaged area, and the amplitude $C_{(x, y)}$ accounts for the spatial variation of the skin, where x is the line number and y is the point number on the line; for example, point (1,1) stands for the first point on the first line scanned.

To fit the image data, a nonlinear least-squares fitting solver was applied to compute the parameters for Eq. (5). The parameters are the same for all the curves in a given figure apart from the amplitude term $C_{(x, y)}$, which represents the spatial variation of skin.

Figures 6 and 7 show the measured peak-to-peak trend line of subjects 1 and 2, respectively. Points from (1,1) to (5,10) are shown in different colors from red to blue. For subject 1 (Figure 6), point (1,10) has the largest amplitude term C_{max} while point (1,1) has the smallest amplitude, C_{min}. From the fitting results of this subject, point (5,7) has the amplitude that is closest to the mean amplitude of the measured 50 points. The positions of these three points are marked in Figure 5. The fitted reduction curves shown in Figure 7 for subject 2 follow the same selection criteria.

Figures 6 and 7 suggest that the occlusion effects can be modeled using time dependent and spatial dependent parameters, which allows us to analyze this THz in vivo image data more meaningfully. It is clear that the greatest change in the THz signal occurs in the first 3 minutes of the occlusion and that after 15 minutes, the reduction rate of the THz signal is smaller.

Table 1 gives the fitted parameters in Eq. (6) for 5 subjects. To avoid overfitting, we give the adequate fitting ranges of the parameter sets with the highest adjusted R^2 (coefficient of determination) for each subject. The table gives the mean and SD of each parameter which may be helpful with fixing the ranges of these parameters for healthy skin in the future.

The fitted signals matched the measured ones well with the adjusted R^2 larger than 0.976 for all 5 subjects. We find

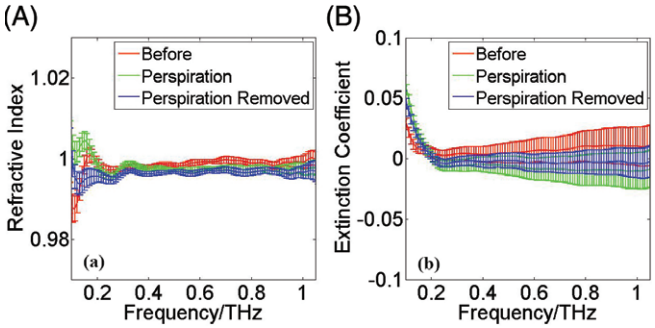

FIGURE 4 (A) Refractive index and (B) extinction coefficient of air, measured before the skin measurement, right after 20 minutes of skin contact and immediately after the perspiration layer was removed

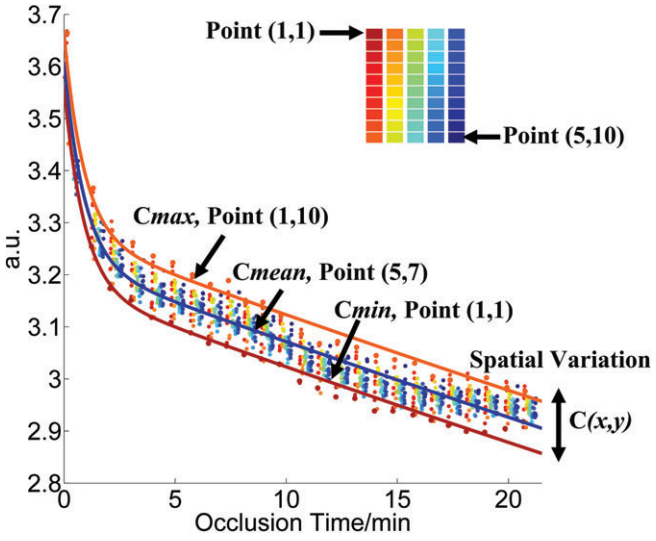

FIGURE 6 The reduction trends of all 50 points on the imaged area and fitted curves of points (1,10), (5,7) and (1,1) of subject 1. The positions of these 3 points are marked in Figure 5

that the amplitude β_2 has the best robustness while the reduction constants τ_1 and τ_2 have relatively larger variation. A possible variable that causes the subject variation on these parameters is the water diffusion coefficient in the occluded skin, which has been studied in nonoccluded skin to vary with position and subjects [14–16]. This coefficient determines how fast the water diffuses in the skin, consequently deciding the skin's reaction to the occlusion. Figure 8 illustrates the best-fitted biexponential functions of subjects 1 to 5 (with the amplitude term $C_{(x,\,y)}$ being 0).

At $t = 0$, the signal amplitude is primarily determined by $\beta_1 + \beta_2$ as the spatial variation term $C_{(x,\,y)}$ accounts for less than 2% of the signal. This value illustrates the initial water concentration in the skin without occlusion effects. Apparently, the forearm skin of subject 2 is the least hydrated among the 5 subjects as the model gives the largest amplitude $\beta_1 + \beta_2$ at $t = 0$. On the contrary, subject 3 has the most hydrated skin. The water diffusion in the SC is driven by the water concentration gradient in the SC [17]: as the occlusion time increases, the hydration gradient decreases and the water concentration of the surface SC saturates to the hydration level at the bottom of the SC [18–20]. From the results shown in Table 1, we find that β_2 and τ_2 in Eq. (6) have much larger values than the other 2 terms. The time constant τ_2 is of the order 200 minutes which is approximately 2 orders of magnitude larger than τ_1. This suggests that the longer the occlusion lasts, the more the fitted signal depends on the second term in Eq. (6); consequently this term represents the hydration level toward the bottom of the stratum corneum. The reduction rates τ_1 and τ_2 determine how fast the skin hydration changes; they are likely to be dominated by the water diffusion coefficient in the occluded human skin.

3.4 | Frequency-domain results

Figure 9 shows how the frequency domain result for one subject changes as the occlusion time increases. As the occlusion time increases, the amplitude ratio M_{mag} decreases. However, the separation between the curves in Figure 9A gradually decreases as the occlusion time increases; the interval is particularly large between 0 and 5 minutes of occlusion. Similarly, the change in the phase, M_{phase}, (Figure 9B) is significant between 0 and 5 minutes

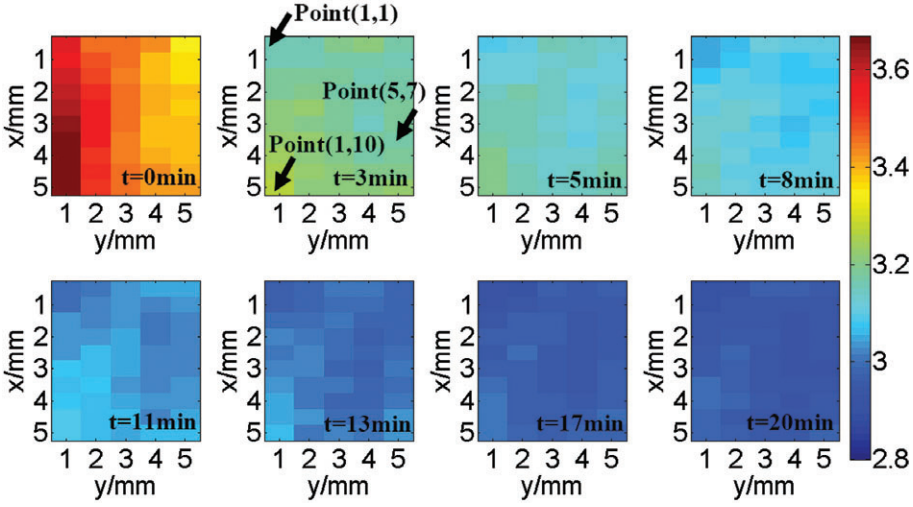

FIGURE 5 Images of an area of skin under occlusion (subject 1)

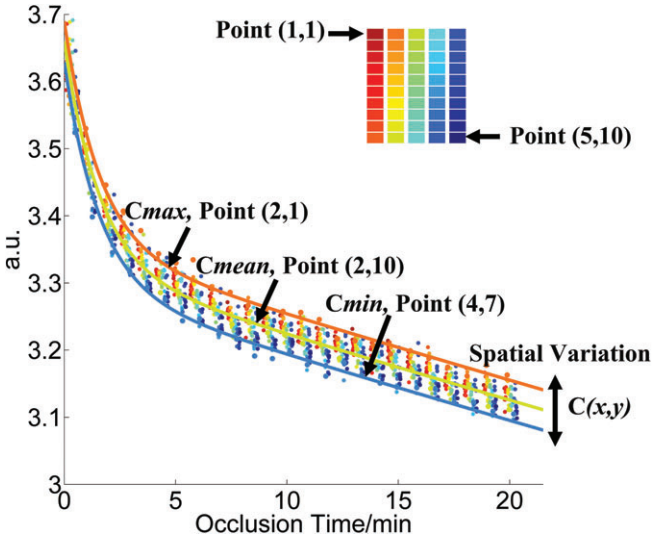

FIGURE 7 The reduction trends of all 50 points on the imaged area and fitted curves of points (2,1), (2,10) and (4,7) of subject 2

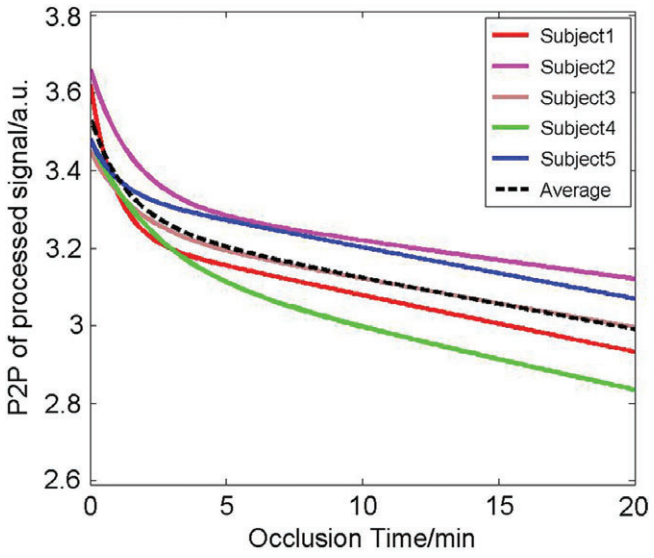

FIGURE 8 Fitted biexponential functions of subject 1 to 5. The black dashed line is the average of all the subjects

of occlusion but it is not evident for the rest of the curves as the error bars then overlap.

Figure 10A,B presents the rapid scan results highlighting the change in refractive index and extinction coefficient, respectively, at 0.2, 0.4 and 0.6 THz for subject 1 as a function of occlusion time. Figure 10C,D presents the same data but normalized by the first point with no occlusion so as to give a percentage change as follows:

$$\%\text{Difference} = \frac{n(t) - n(t=0)}{n(t=0)} \times 100\% \tag{7}$$

After 20 minutes of occlusion, the refractive index increased by 10% to 15% for subject 1. In contrast, the extinction coefficient decreases for all three frequencies as a function of occlusion time.

The underlying cause of the change in the THz time domain signal and amplitude ratio in the frequency domain is the increased water content in the occluded skin [21] as this consequently increases the refractive index (n) and extinction coefficient (κ) of the measured skin. However, the uneven surface of the skin also induces a small air gap between the skin and the imaging window; consequently reducing the accuracy of the measured signals, particularly the high frequency components. A small phase misalignment between sample and reference can lead to large errors in the optical properties extraction [8]: the extinction coefficient is extremely sensitive to the acquired phase. Mathematically, the reduction of M_{mag} suggests an increase in the refractive index of the sample and a decrease in the extinction coefficient. The increase of M_{phase} results in an increase on both refractive index and extinction coefficient [10]. For the occluded skin, the effect of the magnitude reduction of the reflected signal is larger than the effect of phase increase. Moreover, for high frequencies, the scattering effects of THz waves caused by the uneven skin surface may also increase the uncertainty of the measured data [22]. However, the successful modeling of the occlusion effect allows us to remove the occlusion effect from the recorded images, as we now introduce.

4 | PROCESSED SIGNAL RETRIEVAL

To prove the feasibility of the proposed model, Eq. (6) and the parameters in Table 1 are used to retrieve the nonoccluded time domain signal. In Figure 11, all the THz images under occlusion are retrieved relative to the first image. However, scanning the first image also took time, hence Figure 12 gives the images that are retrieved at $t = 0$, that is, the nonoccluded state and time at which the first point of image 1 was measured. Both color bars in the 2 figures are the same as the one used in Figure 5. By this method we have shown that our model can be used to retrieve the THz

TABLE 1 Bioexponential function parameters range for 5 subjects

Subject	β_1	τ_1 (min)	β_1	τ_1 (min)	$C_{(x,y)}$	$\overline{R^2}$
1	0.37 ±0.01	0.93 ±0.08	3.22 ±0.00	208.53 ±4.75	0 ±0.02	>0.976
2	0.33 ±0.01	1.36 ±0.06	3.34 ±0.00	293.12 ±3.90	0 ±0.02	>0.979
3	0.20 ±0.01	1.62 ±0.13	3.25 ±0.01	246.97 ±6.87	0 ±0.03	>0.984
4	0.32 ±0.01	2.35 ±0.14	3.16 ±0.01	184.46 ±5.21	0 ±0.02	>0.991
5	0.13 ±0.01	1.06 ±0.10	3.36 ±0.00	242.10 ±1.76	0 ±0.03	>0.982

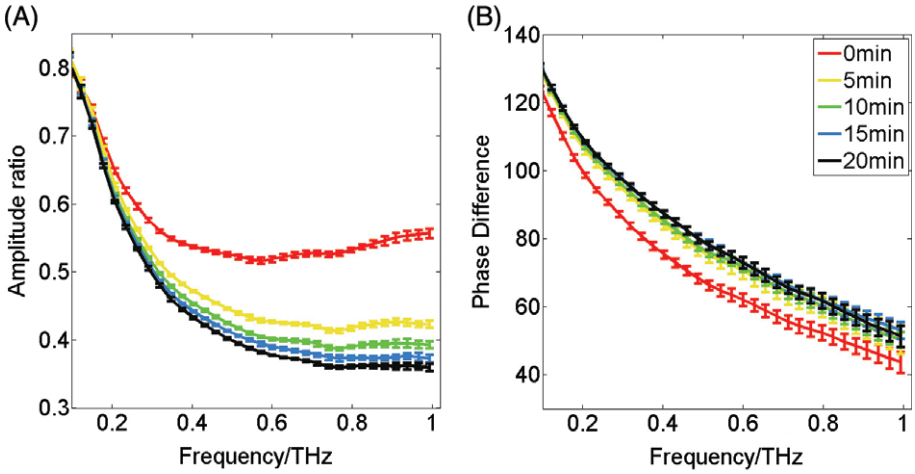

FIGURE 9 The spectrum of the amplitude ratio and phase difference of the sample and reference at 5 minutes intervals during 20 minutes of occlusion

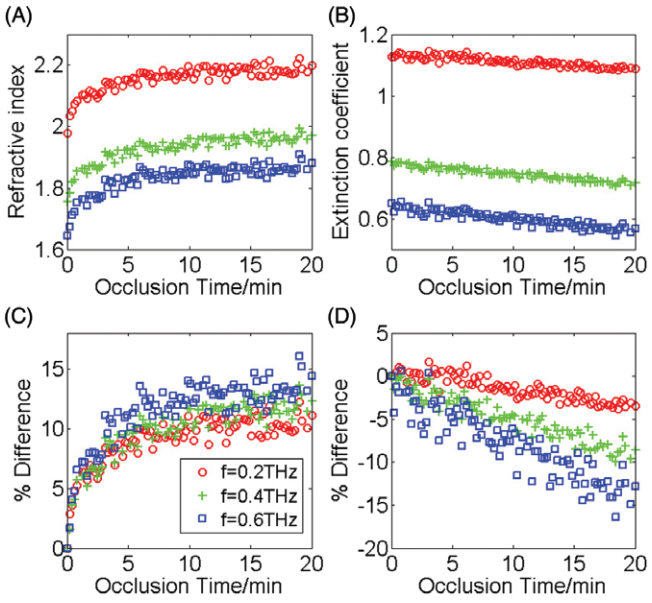

FIGURE 10 The change in (A) refractive index, (B) extinction coefficient, (C) normalized refractive index, (D) normalized extinction coefficient at 0.2, 0.4 and 0.6 THz as a function of the occlusion time for subject 1

images to the nonoccluded state which could help improve the contrast of THz images.

In summary, the influence of imaging window in in vivo THz measurements can be described and modeled by a biexponential function with time and spatial-dependent parameters. This helps trace back the normal skin properties with the influence of imaging widow and imaging time removed.

5 | SUMMARY

In this article, we have discussed the variables that may affect the THz response during in vivo human skin measurements and studied the effects of occlusion. We have used a biexponential function to model and retrospectively account for the changes in the THz signal. The fitted parameters in the model contain information about the water concentration at the surface and deep within the skin. The act of placing skin on the imaging window leads to subtle changes at the skin surface, the dominant factor being skin occlusion which in turn causes an increase of water concentration in the stratum corneum. Our experimental results show that THz light is very sensitive to the change of water concentration underneath the skin and the first 3 minutes

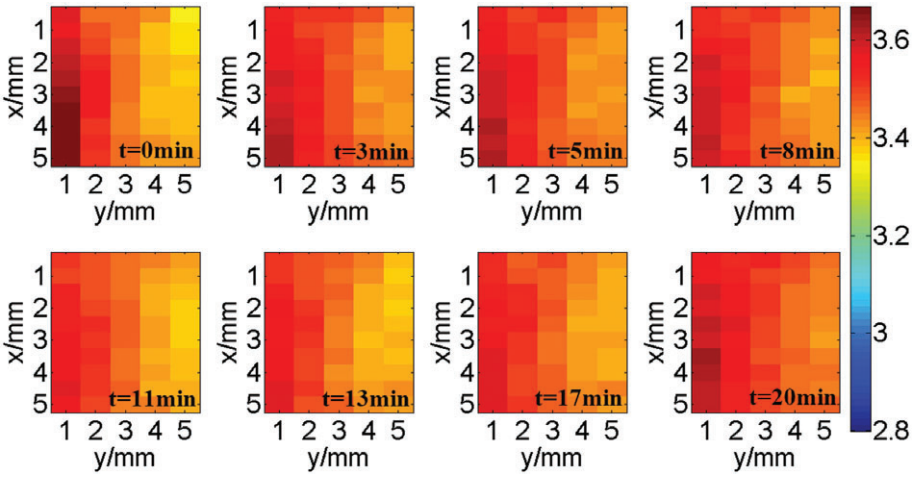

FIGURE 11 Retrieving all the images of subject 1 to the first image. The colorbar is the same as in Figure 5

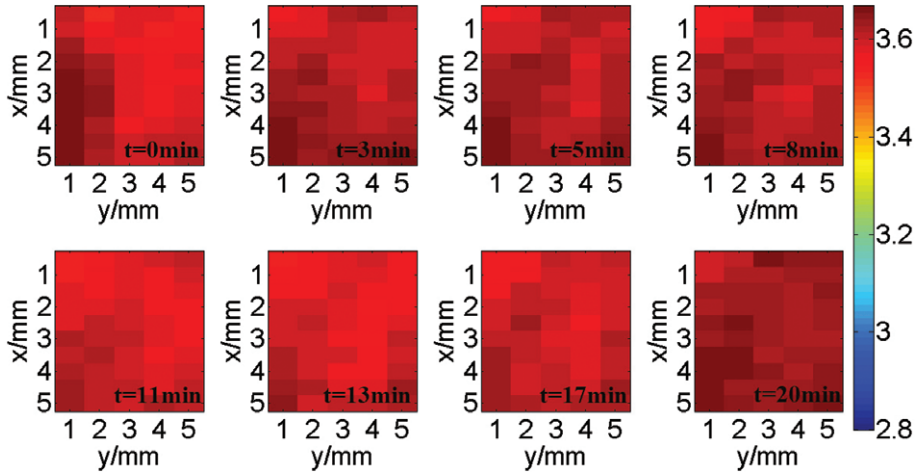

FIGURE 12 Retrieving all the images of subject 1 to the nonoccluded state (ie, the first pixel of image 1). The colorbar is the same as in Figure 5

show the biggest effect on the results. The occlusion of the skin also has effects on the THz spectrum and optical properties: it leads to a reduction on the amplitude of measured THz signal and a small increase in the phase, that consequently causes changes in refractive index and extinction coefficient.

Occlusion measurements of human skin offer distinctive features and functions for skin assessment and percutaneous studies. In one example, the type of skin damage has been identified by analyzing occlusion curves as measured by capacitive contact imaging [20]. Occlusion effects can also help enhance percutaneous absorption of most chemicals [23] and help with the recovery of hypertrophic scars and keloids [24]. Based on the work presented herein, coupled with the aforementioned capabilities of existing occlusion tests, in vivo THz reflection spectroscopy could be used to noninvasively observe water motion in human skin and monitor the effects of topical chemical treatments.

ACKNOWLEDGMENTS

The authors would like to thank the research grants council of Hong Kong (Project numbers 415313 and 14205514) and the Hong Kong PhD Fellowship award for partial support of this work.

AUTHOR BIOGRAPHIES

Please see Supporting Information online.

REFERENCES

[1] S. Fan, Y. He, B. S. Ung, E. Pickwell-MacPherson, *J. Phys. D Appl. Phys.* **2014**, *47*, 374009.
[2] S. Fan, B. S. Ung, E. P. Parrott, V. P. Wallace, E. Pickwell-MacPherson, *J. Biophotonics* **2016**.
[3] G. G. Hernandez-Cardoso, S. C. Rojas-Landeros, M. Alfaro-Gomez, A. I. Hernandez-Serrano, I. Salas-Gutierrez, E. Lemus-Bedolla, A. R. Castillo-Guzman, H. L. Lopez-Lemus, E. Castro-Camus, *Sci. Rep.* **2017**, *7*, 42124.
[4] N. Bajwa, J. Au, R. Jarrahy, S. Sung, M. C. Fishbein, D. Riopelle, D. B. Ennis, T. Aghaloo, M. A. St John, W. S. Grundfest, Z. D. Taylor, *Biomed. Opt. Express* **2017**, *8*, 460.
[5] B. E. Cole, R. M. Woodward, D. A. Crawley, V. P. Wallace, D. D. Arnone, M. Pepper, *Photonics* **2001**, 1.
[6] K. I. Zaytsev, A. A. Gavdush, N. V. Chernomyrdin, S. O. Yurchenko, *IEEE Trans. Terahertz Sci. Technol.* **2015**, *5*, 817.
[7] S. Huang, P. C. Ashworth, K. W. Kan, Y. Chen, V. P. Wallace, Y.-T. Zhang, E. Pickwell-MacPherson, *Opt. Express* **2009**, *17*, 3848.
[8] S. Fan, E. P. Parrott, B. S. Ung, E. Pickwell-MacPherson, *Photonics Res.* **2016**, *4*, A29.
[9] R. M. Woodward, B. E. Cole, V. P. Wallace, R. J. Pye, D. D. Arnone, E. H. Linfield, M. Pepper, *Phys. Med. Biol.* **2002**, *47*, 3853.
[10] X. Chen, E. P. Parrott, B. S. Ung, E. Pickwell-MacPherson, *IEEE Trans. Terahertz Sci. Technol.* DOI: 10.1109/TTHZ.2017.2722981
[11] R. Roy, D. K. Agrawal, H. A. McKinstry, *Ann. Rev. Mater. Sci.* **1989**, *19*, 59.
[12] E. Pickwell, B. E. Cole, A. J. Fitzgerald, V. P. Wallace, M. Pepper, *Appl. Phys. Lett.* **2004**, *84*, 2190.
[13] H. J. Liebe, G. A. Hufford, T. Manabe, *Int. J. Inf. Millimeter Waves* **1991**, *12*, 659.
[14] D. A. Schwindt, K. P. Wilhelm, H. I. Maibach, *J. Invest. Dermatol.* **1998**, *111*, 385.
[15] S. Bielfeldt, V. Schoder, U. Ely, A. Van Der Pol, J. De Sterke, K. P. Wilhelm, *Int. J. Cosmet. Sci.* **2009**, *31*, 479.
[16] F. Pirot, E. Berardesca, Y. N. Kalia, M. Singh, H. I. Maibach, R. H. Guy, *Pharm. Res.* **1998**, *15*, 492.
[17] I. H. Blank, J. Moloney, A. G. Emslie, I. Simon, C. Apt, *J. Invest. Dermatol.* **1984**, *82*, 188.
[18] M. Egawa, T. Hirao, M. Takahashi, *Acta Derm. Venereol.* **2007**, *87*, 4.
[19] A. K. Dabrowska, C. Adlhart, F. Spano, G. M. Rotaru, S. Derler, L. Zhai, N. D. Spencer, R. M. Rossi, *Biointerphases* **2016**, *11*, 031015.
[20] W. Pan, X. Zhang, M. Lane, P. Xiao, *Int. J. Cosmet. Sci.* **2015**, *37*, 395.
[21] K. Ryatt, M. Mobayen, J. Stevenson, H. Maibach, R. Guy, *Br. J. Dermatol.* **1988**, *119*, 307.
[22] D. B. Bennett, W. Li, Z. D. Taylor, W. S. Grundfest, E. R. Brown, *IEEE Sens. J.* **2011**, *11*, 1253.
[23] H. Zhai, H. I. Maibach, *Skin Pharmacol. Physiol.* **2001**, *14*(1).
[24] B. Berman, O. A. Perez, S. Konda, B. E. Kohut, M. H. Viera, S. Delgado, D. Zell, Q. Li, *Dermatol. Surg.* **2007**, *33*, 1291.

How to cite this article: Sun Q, Parrott EPJ, He Y, Pickwell-MacPherson E. In vivo THz imaging of human skin: Accounting for occlusion effects. *J. Biophotonics*. 2018;11:e201700111. https://doi.org/10.1002/jbio.201700111